Electronic Supplementary Information (ESI)

Asymmetric Supercapacitor with Excellent Cycling Performance Realized by Hierarchical Porous $NiGa_2O_4$ Nanosheets

Shude Liu[a], Kwan San Hui[b,*], Kwun Nam Hui[c,*], Hai-Feng Li[c], Kar Wei Ng[c], Jincheng Xu[c], Zikang Tang[c], and Seong Chan Jun[a,*]

[a]Nano-Electro Mechanical Device Laboratory, School of Mechanical Engineering, Yonsei University, Seoul 120-749, South Korea

[b]School of Mathematics, University of East Anglia, Norwich, NR4 7TJ, United Kingdom

[c]Institute of Applied Physics and Materials Engineering, University of Macau, Avenida da Universidade, Macau, China.

*E-mail: bizhui@umac.mo (Kwun Nam Hui)

*E-mail: k.hui@uea.ac.uk (Kwan San Hui)

*E-mail: scj@yonsei.ac.kr (Seong Chan Jun)

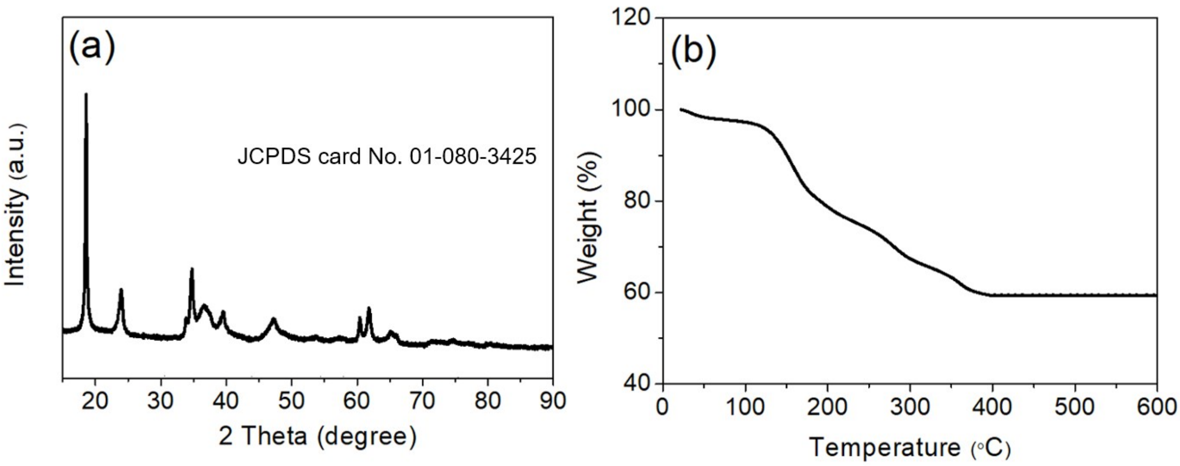

Figure S1. (a) XRD pattern and (b) TGA curve of the as-prepared NiGa-precursor.

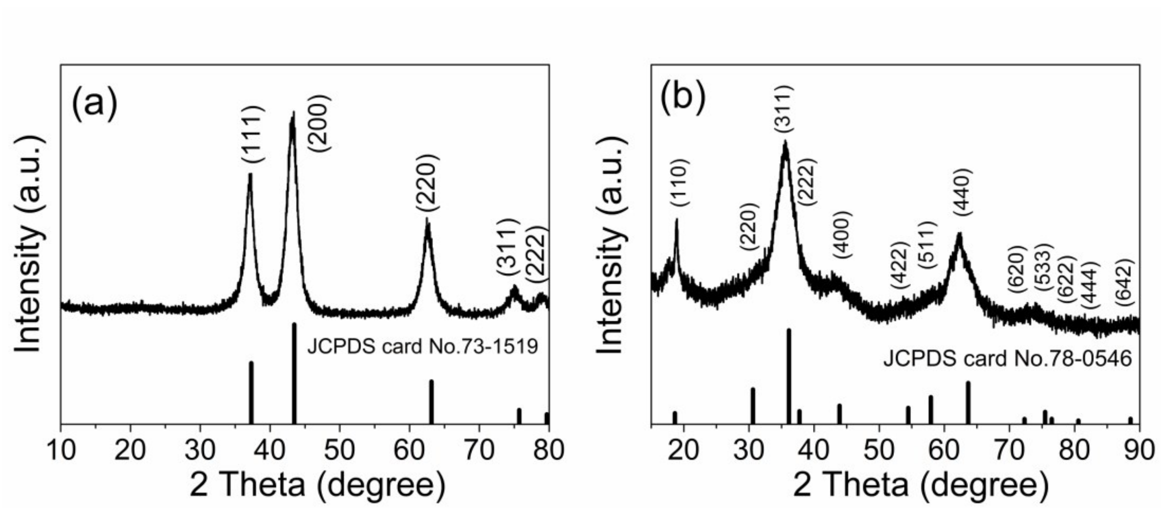

Figure S2. Typical XRD patterns of the (a) NiO and (b) $NiGa_2O_4$ samples.

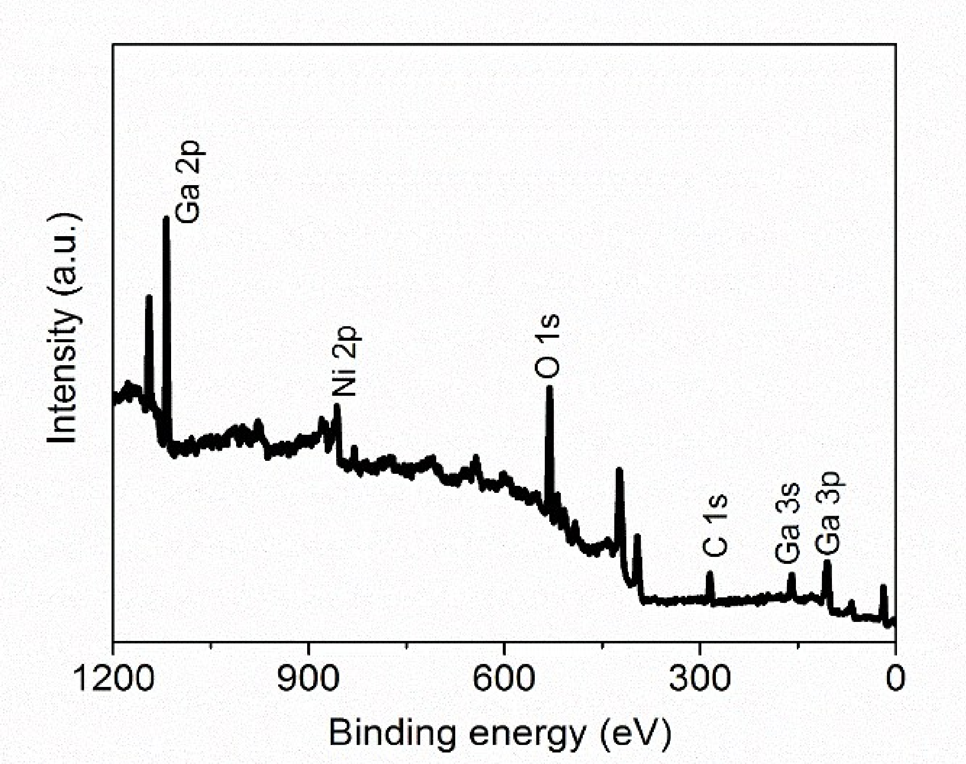

Figure S3. XPS general spectra of the $NiGa_2O_4$ nanosheets.

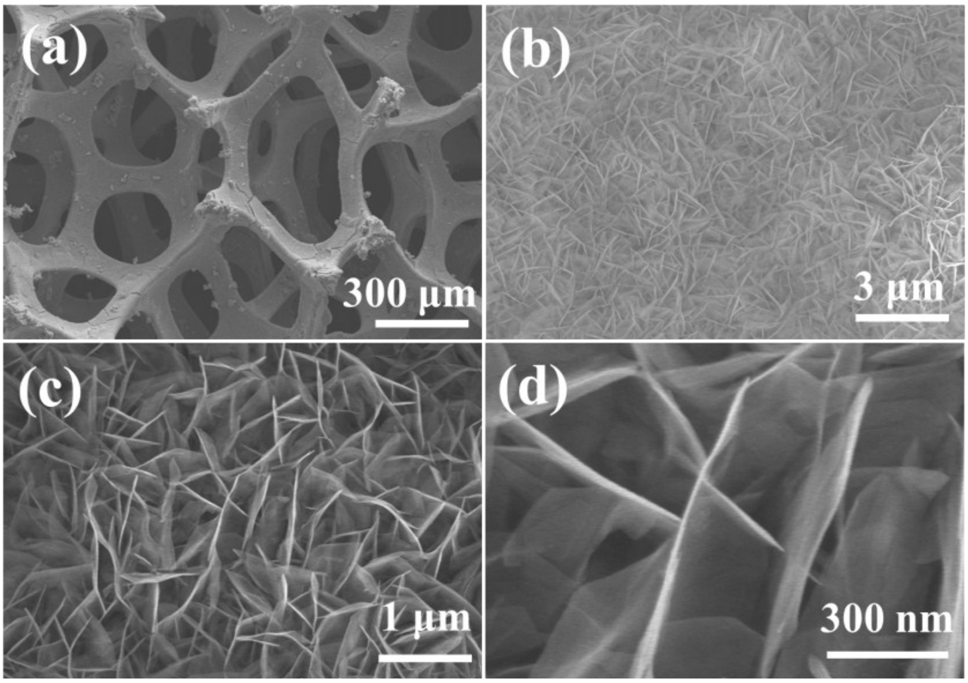

Figure S4. SEM images at high and low magnification of the $NiGa_2O_4$-4 h nanosheets.

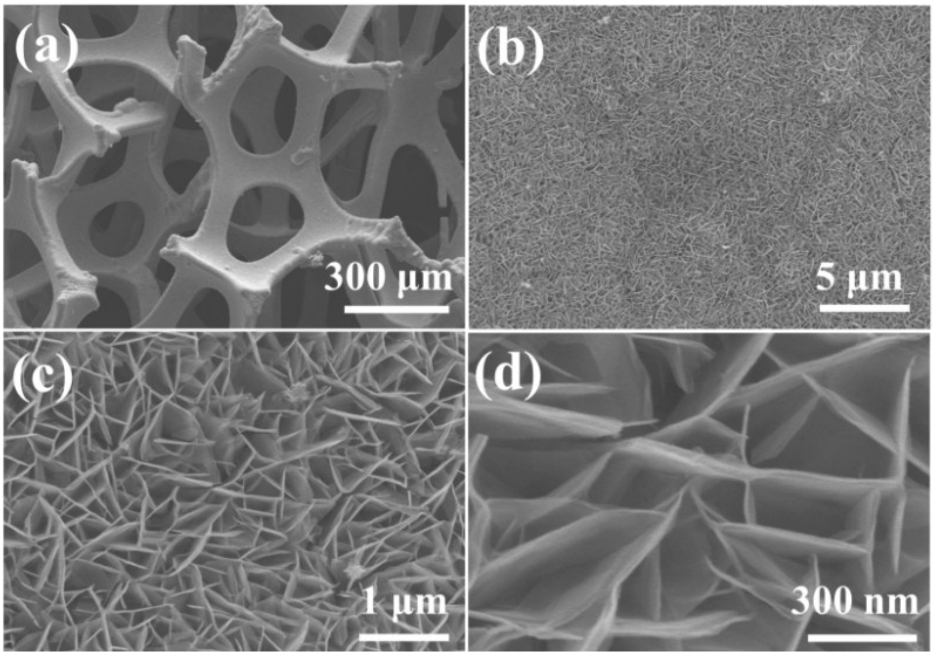

Figure S5. SEM images at high and low magnification of the $NiGa_2O_4$-8 h nanosheets.

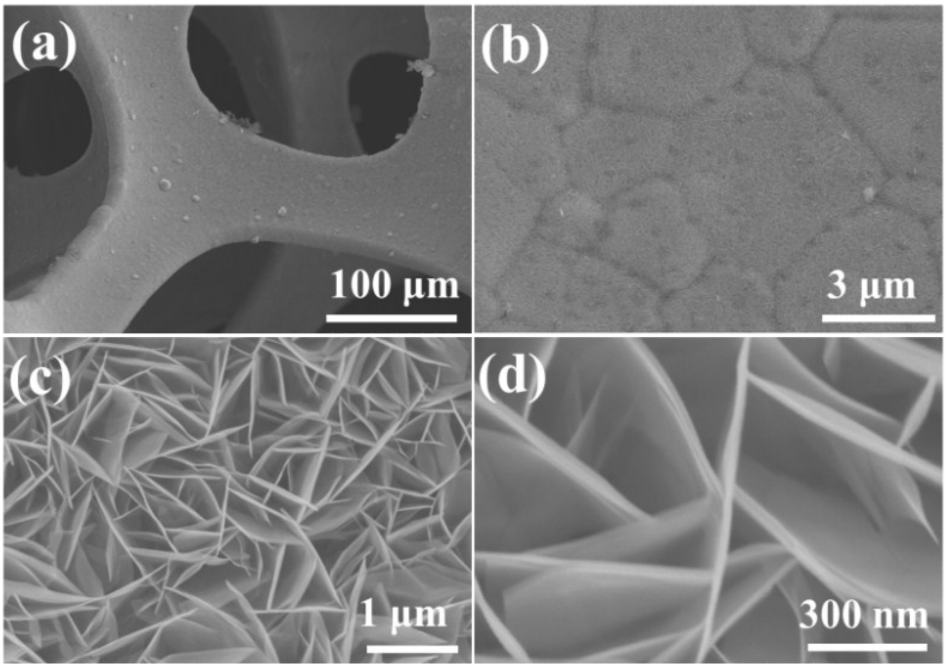

Figure S6. SEM images at high and low magnification of the $NiGa_2O_4$-12 h nanosheets.

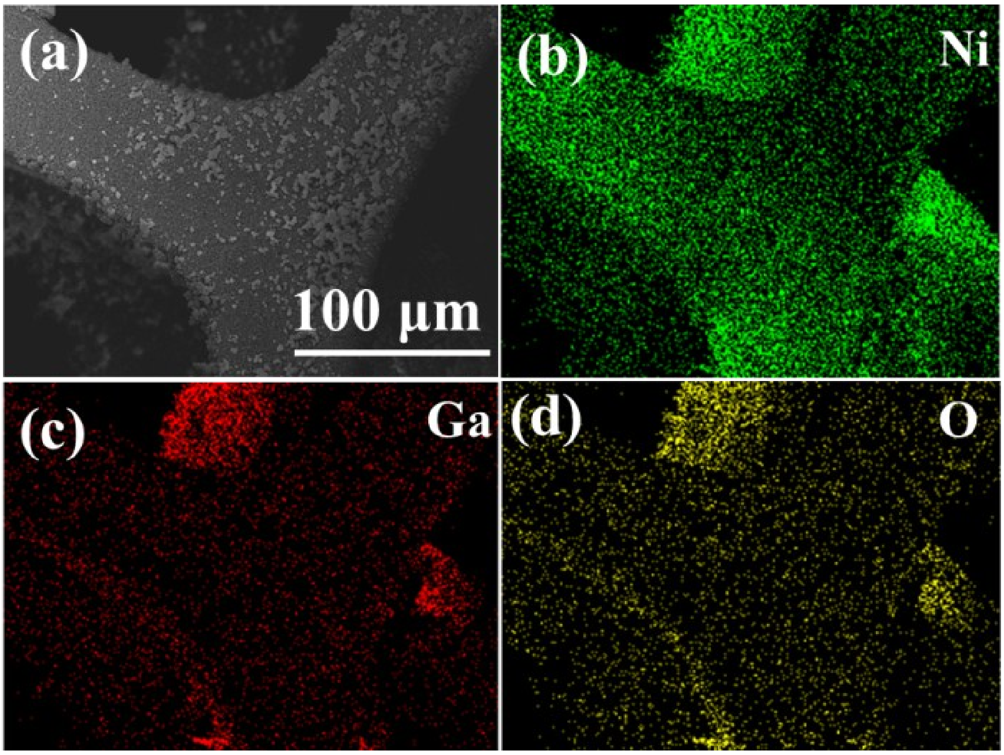

Figure S7. (a) SEM image of the $NiGa_2O_4$-12 h nanosheets on Ni foam and (b–d) the corresponding elemental mapping of Ni, Ga, and O.

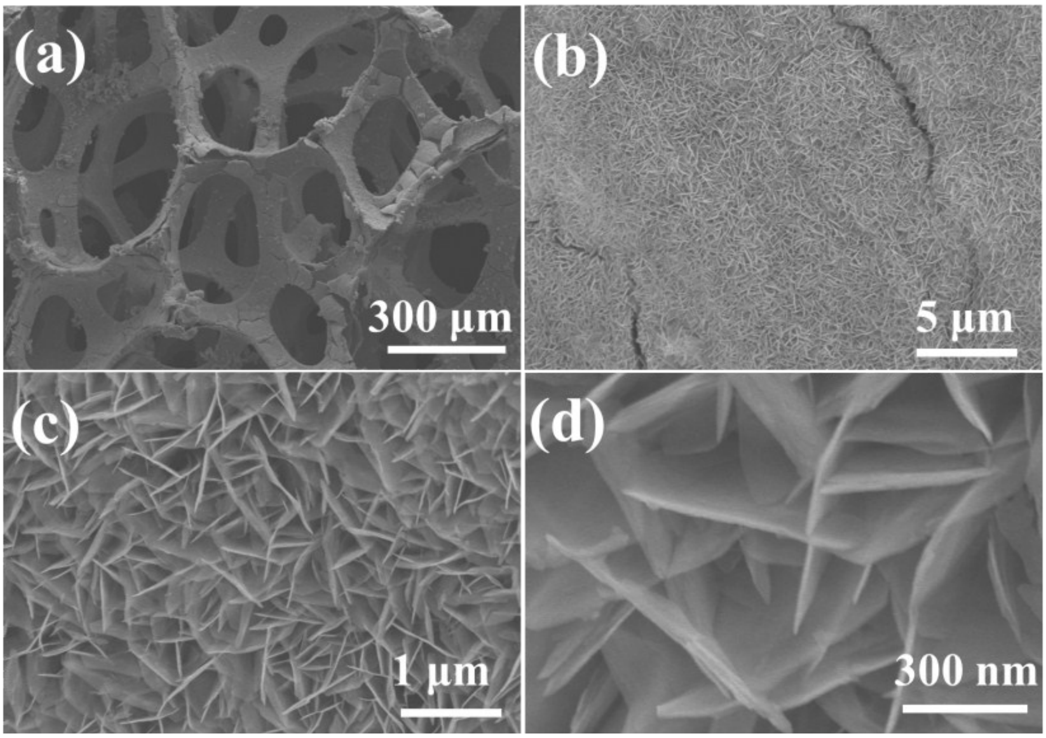

Figure S8. SEM images at high and low magnification of the $NiGa_2O_4$-16 h nanosheets.

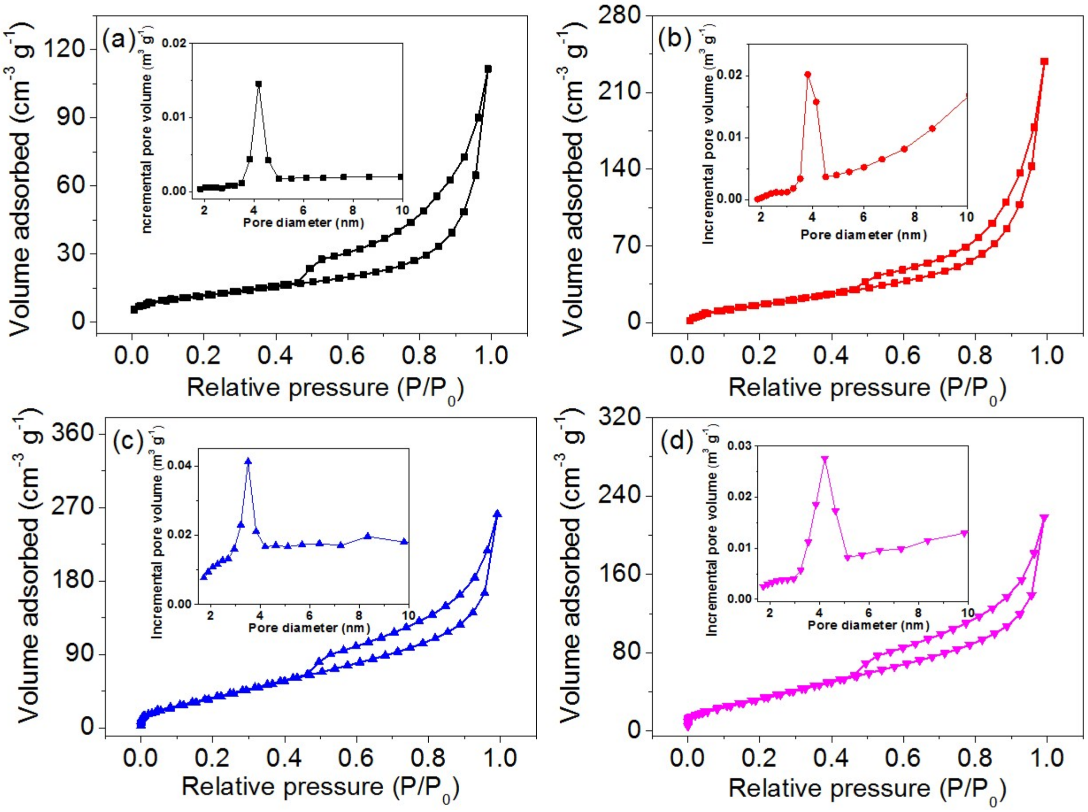

Figure S9. Nitrogen adsorption–desorption isotherms and pore size distribution curves of (a) $NiGa_2O_4$-4 h, (b) $NiGa_2O_4$-8 h, (c) $NiGa_2O_4$-12 h, and (d) $NiGa_2O_4$-16 h samples.

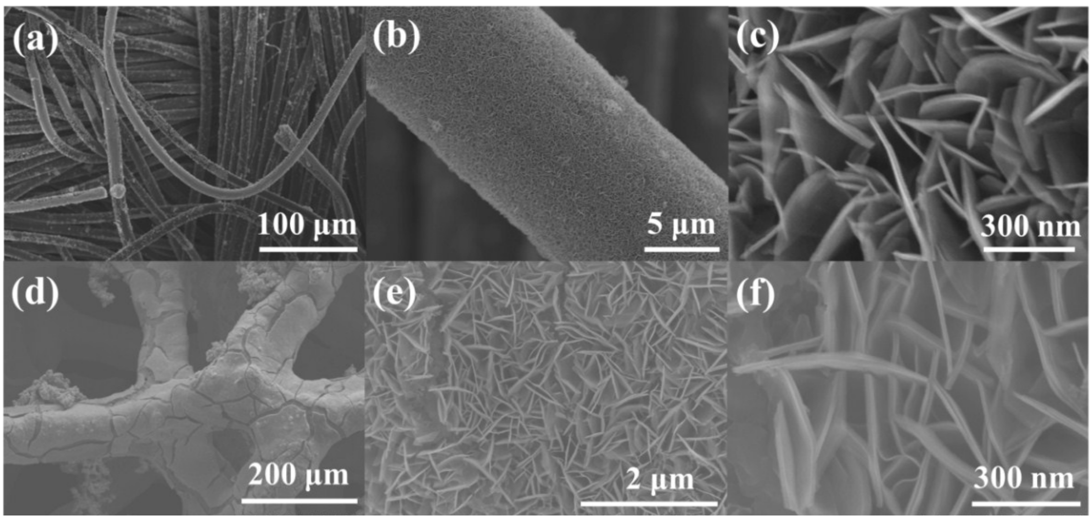

Figure S10. SEM images of the $NiGa_2O_4$-12 h on the different substrates: (a–c) C fiber; (d–f) Cu foam.

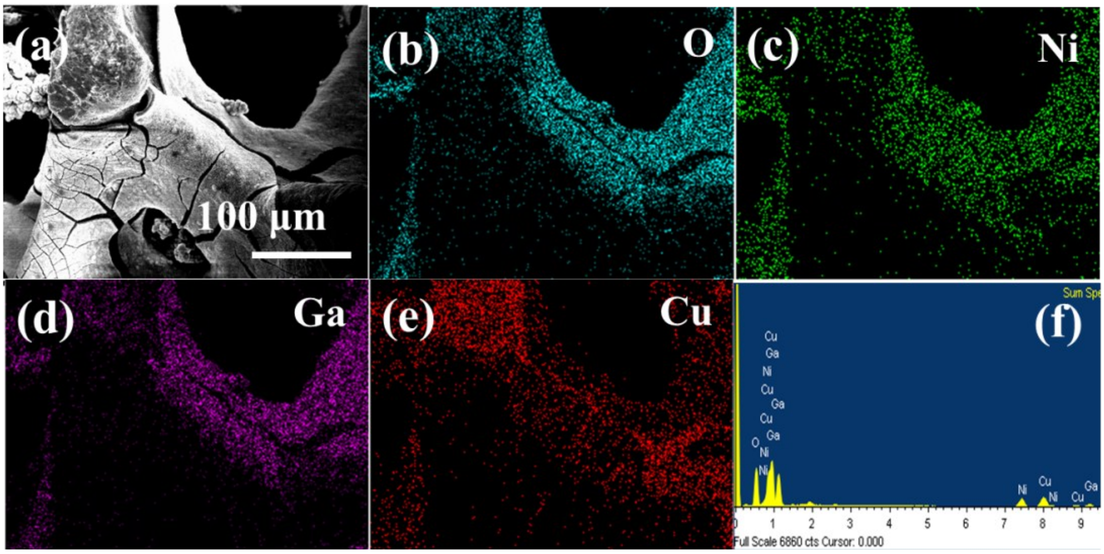

Figure S11. (a–e) Mapping results from the $NiGa_2O_4$-12 h nanosheets on Cu foam and (f) the corresponding EDS spectrum.

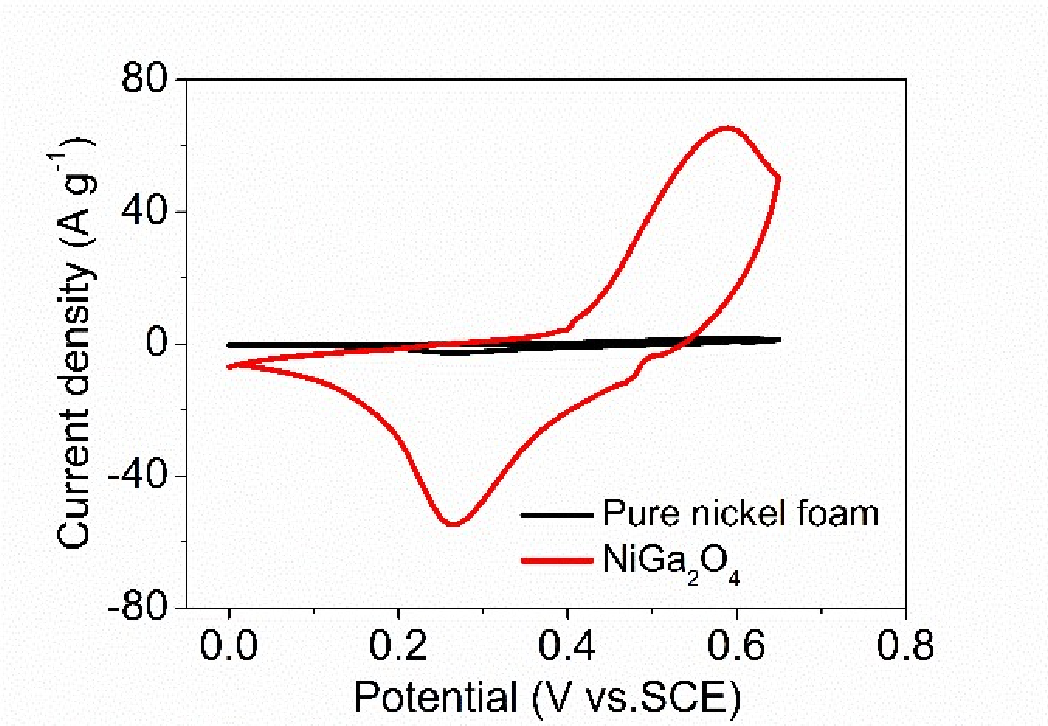

Figure S12. CV curves of the $NiGa_2O_4$-12 h nanosheets and pure Ni foam electrodes obtained at a scan rate of 50 mV s^{-1}.

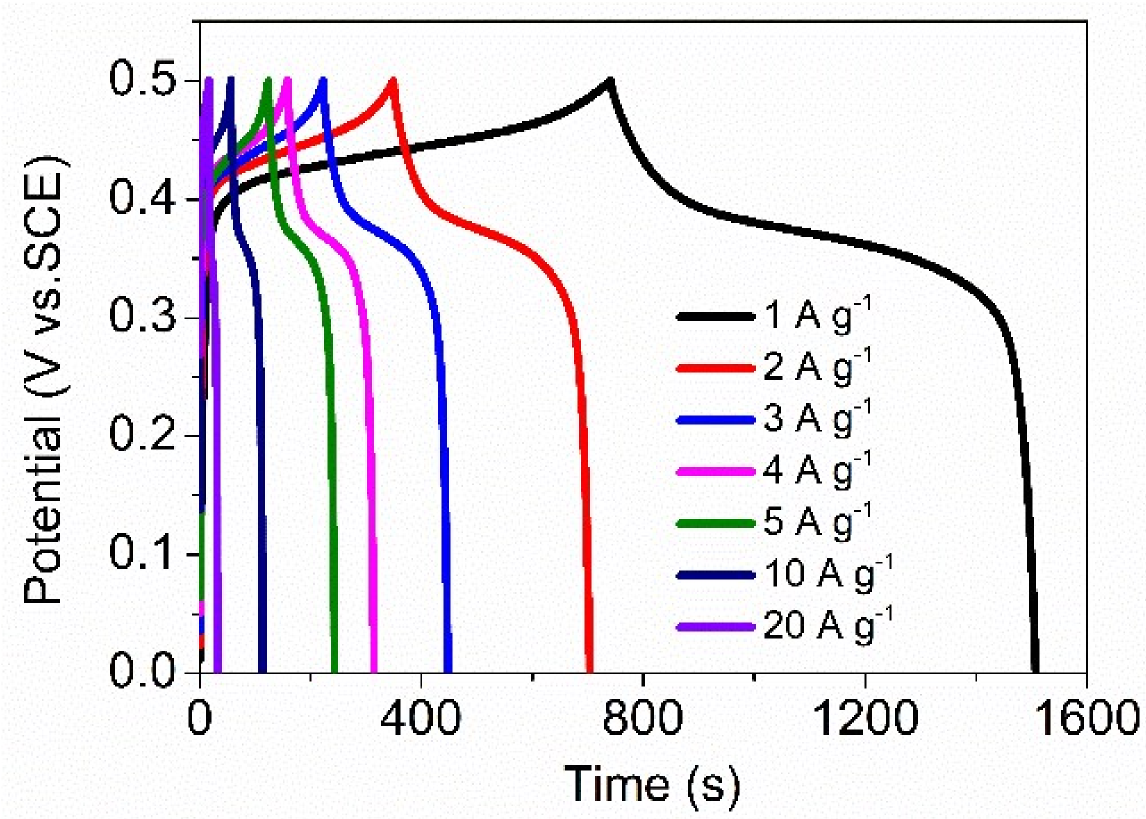

Figure S13. GCD curves of $NiGa_2O_4$-12 h sample at different current densities from 1 to 20 A g^{-1}.

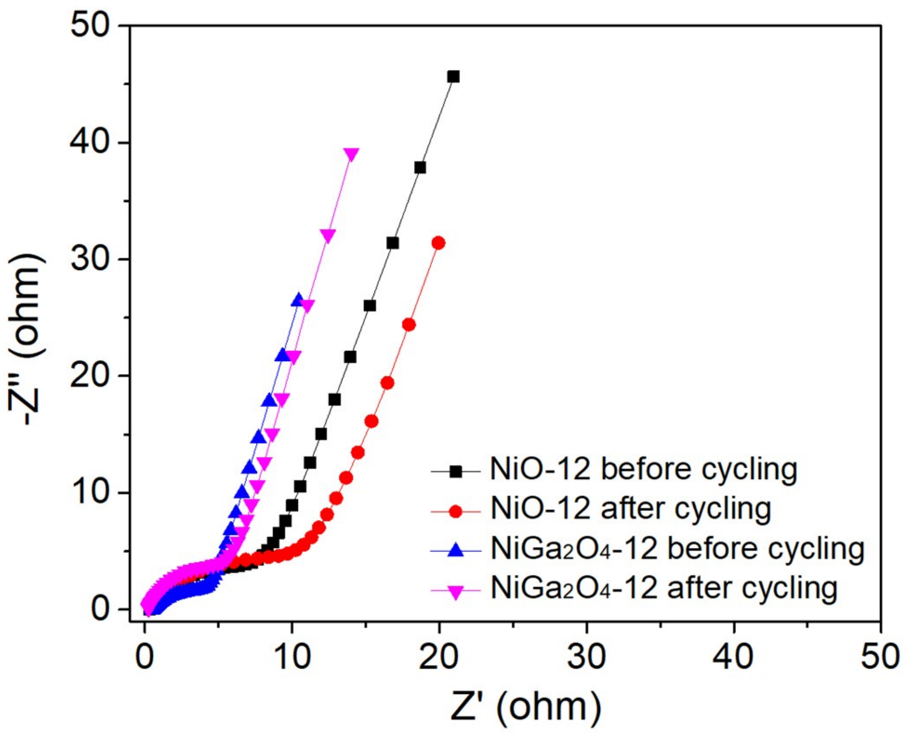

Figure S14. EIS curves of the NiO-12 h and NiGa2O4-12 h electrodes before and after the cycling test.

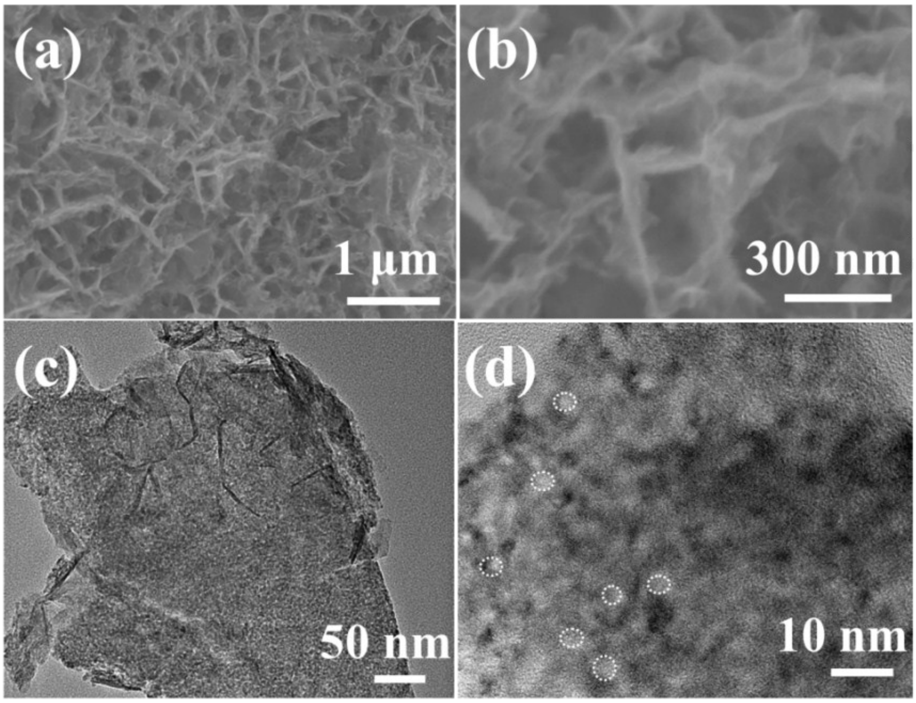

Figure S15. SEM and TEM images of $NiGa_2O_4$-12 h nanosheet electrode after cycle test: (a–b) SEM image; (c) low-magnification TEM image; (d) HRTEM image.

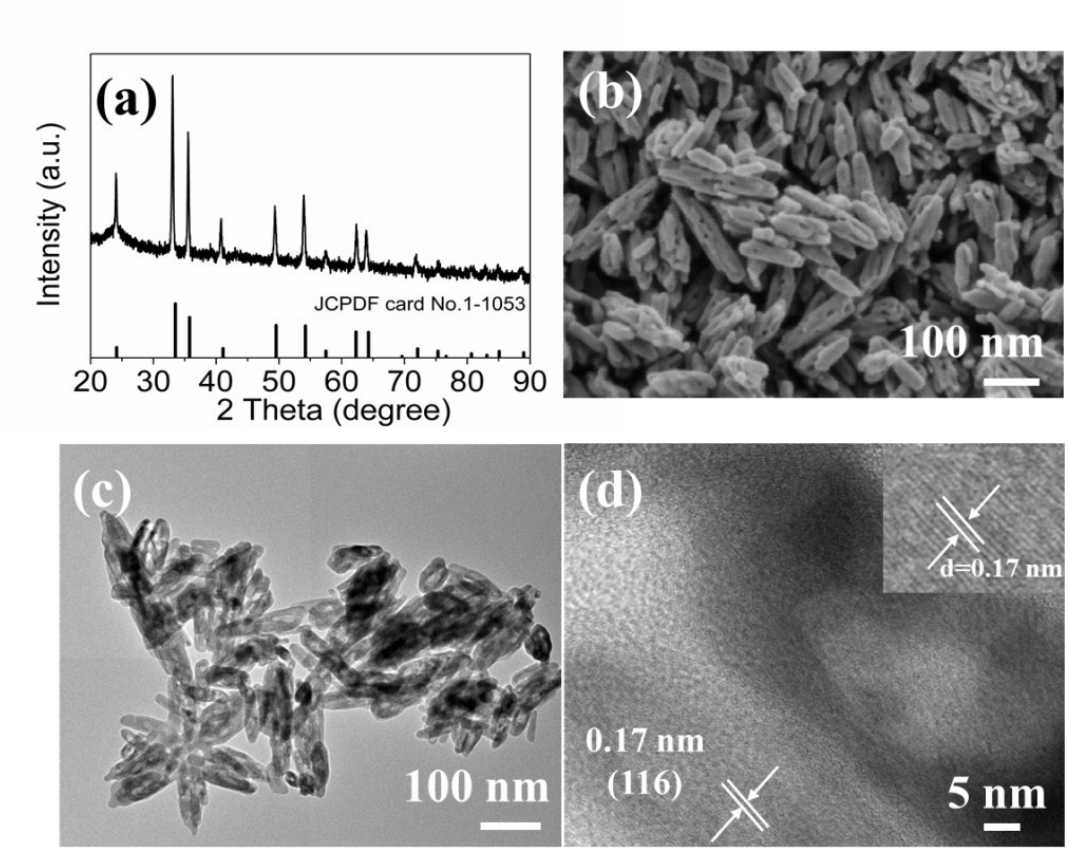

Figure S16. Structural and morphology characterization of spindle-like Fe_2O_3: (a) XRD pattern; (b) SEM image; (c–d) TEM images at different resolutions.

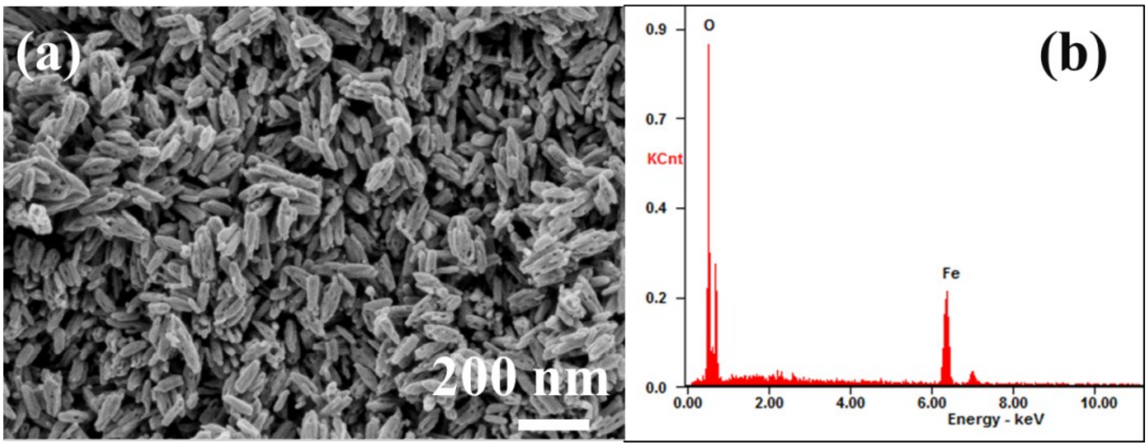

Figure S17. (a) SEM image of spindle-like Fe_2O_3; (b) corresponding EDX spectra.

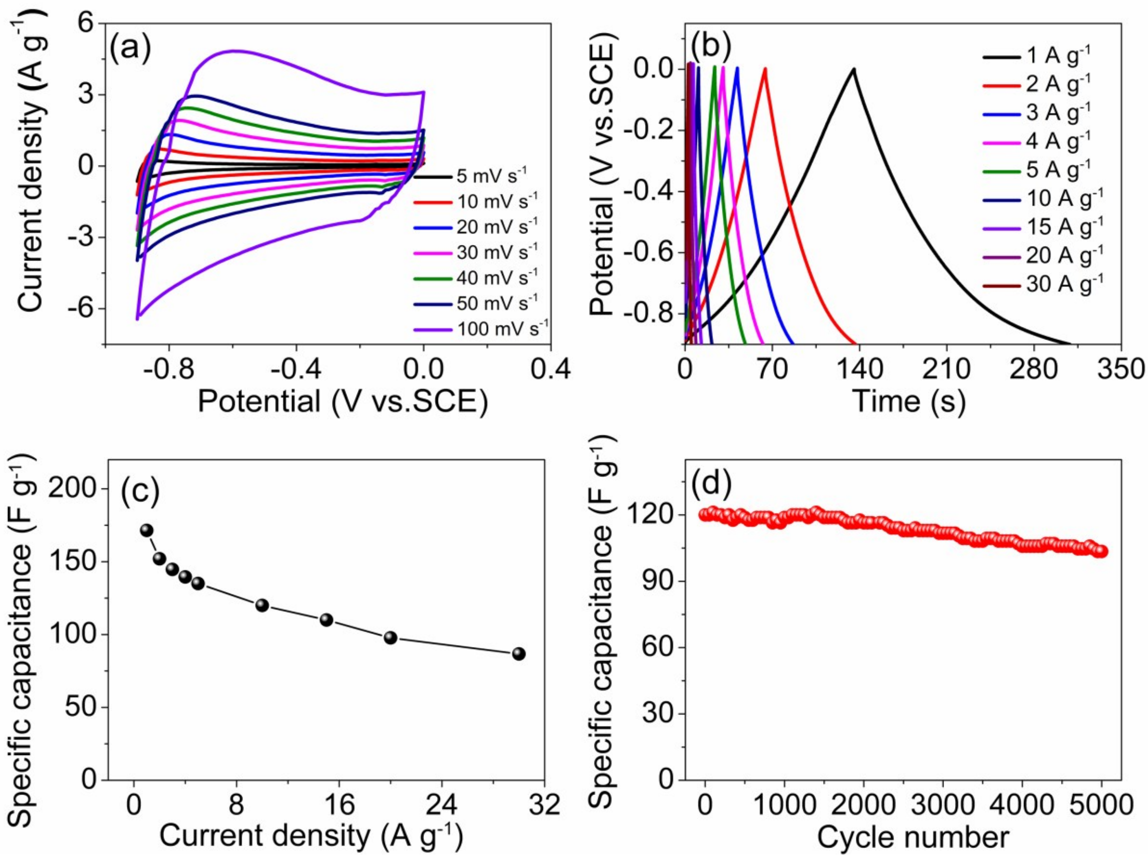

Figure S18. Electrochemical properties of Fe_2O_3: (a) CV curves. (b) Charge–discharge voltage profiles. (c) Specific capacitance at different current densities. (d) Cycling performance at a current density of 10 A g^{-1}.

To study the electrochemical properties of the as-prepared spindle-like Fe_2O_3, the CV GCD cycling, and EIS measurements are performed in a 6 M KOH solution. **Figure S18a** shows the CV curves of Fe_2O_3 electrode at various scan rates range from 5 to 100 mV S^{-1} in the potential window of −0.9–0 V vs. SCE. The similar rectangular shape of CV curves is manifested by the Faradaic behavior of Fe_2O_3, which might arise from a reversible Fe^{3+}/Fe^{2+} couple. The peak current increases with an insignificant change in the CV shape, although the scan rate increases to 100 mV s^{-1}, which reveals its good electrochemical reversibility and high rate capability. GCD measurements are conducted in a potential range of −0.9–0 V at various current densities ranging from 1 to 30 A g^{-1}, as displayed in **Figure S18b**. The specific capacitance corresponded to 171.5 F g^{-1} at a current density of 1 A g^{-1} and remains at 86.7 F g^{-1} at a high current density of 30 A g^{-1} (**Figure S18c**). In particular, the stable specific capacitance of 103 F g^{-1} can be retained for the spindle-like Fe_2O_3 after 5,000 cycles at 10 A g^{-1} with capacitance retention of almost 86% (**Figure S18d**), indicating a good electrochemical stability. The outstanding rate capability and electrochemical stability could be attributed to the one-dimensional spindle structure, which is in favor of fast ion diffusion and provides a short transport distance. In order to further confirm the excellent performance of the spindle-like Fe_2O_3 electrode.

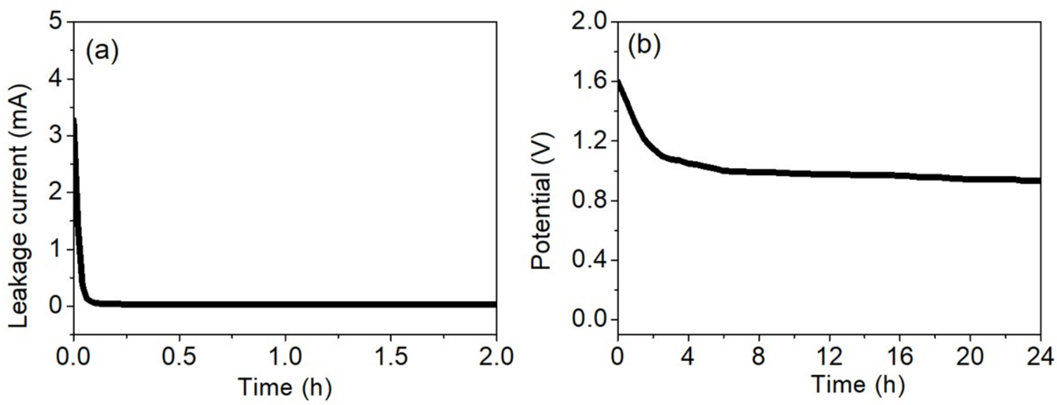

Figure S19. (a) Leakage current and (b) self-discharge curves of the $NiGa_2O_4$-12 h//Fe_2O_3 ASC device.

Table S1. Comparison of cyclic performances between the $NiGa_2O_4$ and previous reports on Ni-based oxides/hydroxides/sulfides.

Material	The correspondin g current density	Capacitance retention (cycles)	Ref
$Ni(OH)_2$ nanosheets	5 A g^{-1}	75% (3,000)	S1
$Ni(OH)_2$/RGO/$Ni(OH)_2$ films	20 mA cm^{-2}	95.3% (3,000)	S2
CNT@$Ni(OH)_2$ nanosheets	8 A g^{-1}	92% (1,000)	S3
MnCo-LDH@$Ni(OH)_2$ core–shell heterostructures	20 A g^{-1}	90.9% (5,000)	S4
NiO nanotubes	2 A g^{-1}	93.2% (10,000)	S5
α-Fe_2O_3 nanorod/NiO nanosheet	1 mA cm^{-2}	96.2% (3,000)	S6
$NiCo_2O_4$ nanowire@$CoMoO_4$ nanoplate	10 mA cm^{-2}	77.7% (1,000)	S7
$ZnCo_2O_4$@$Ni_xCo_{2x}(OH)_{6x}$ core/shell nanowires	20 mA cm^{-2}	85.6% (2,000)	S8
Ni-Co-S nanoparticles/graphene	6 A g^{-1}	90% (8,000)	S9
$NiCo_2O_4$ nanowire@Ni_3S_2 nanosheet	2 A g^{-1}	93.3% (10,000)	S10
$NiGa_2O_4$ nanosheets	20 A g^{-1}	102.4% (10,000)	Present work

Table S2. Refined room-temperature structural parameters of NiO and $NiGa_2O_4$ compounds as well as the calculated shortest bond lengths (Å) and the goodness of fit.

NiO (cubic, space group *Fm-3m* (NO.225), Z = 4)					
$a = b = c$ (Å)			4.1921(15)	4.1921(15)	4.1921(15)
α, β, γ (°)			90	90	90
Atom	Site	x	y	z	B (Å^2)
Ni	4*a*	0.00	0.00	0.00	2.03(4)
O	4*b*	0.50	0.50	0.50	1.98(9)
Shortest Ni-Ni: 2.9643(1) Å					
Shortest Ni-O: 2.0997(1) Å					
R_B = 2.34, R_F = 1.20, and χ^2 = 1.80					
$NiGa_2O_4$ (cubic, space group *Fd-3m* (NO.227), Z = 8)					
$a = b = c$ (Å)			8.2977(81)	8.2977(81)	8.2977(81)
α, β, γ (°)			90	90	90
Atom	Site	x	y	z	B (Å^2)
Ni	16*c*	0.00	0.00	0.00	0.73(4)
Ga1	16*c*	0.00	0.00	0.00	1.06(5)
Ga2	8*b*	0.375	0.375	0.375	1.06(5)
O	32*e*	0.253(1)	0.253(1)	0.253(1)	0.50(1)
Shortest Ni(Ga1)-Ni(Ga1): 2.9338(1) Å					
Shortest Ni(Ga1)-O: 2.0961(1) Å					
Shortest Ga2-Ga2: 3.5931(1) Å					
Shortest Ga2-O: 1.7535(1) Å					
R_B = 13.57, R_F = 9.04, and χ^2 = 1.21					

Table S3. Comparison of cyclic performances between the $NiGa_2O_4$//Fe_2O_3 ASC device and the previous reports

Device	Corresponding current density/scan rate	Capacitance retention (cycles)	Ref
$MnCo_2O_4$@$Ni(OH)_2$//AC	6 A g^{-1}	90% (2,500)	S11
N-doped cellulose @NiCo-LDH//N-doped cellulose	10 A g^{-1}	74.4% (5,000)	S12
$(Ni, Co)_{0.85}Se$//graphene	20 mA cm^{-2}	85% (10,000)	S13
Cu_2O/$CuMoO_4$//AC	5 A g^{-1}	86.6% (3,000)	S14
CoNi-LDH//FeOOH	100 mV s^{-1}	92.3% (3,000)	S15
$NiGa_2O_4$//Fe_2O_3	10 A g^{-1}	94.3% (10,000)	Present work

References

1. X. Xiong, D. Ding, D. Chen, G. Waller, Y. Bu, Z. Wang and M. Liu, Nano Energy, 2015, 11, 154-161.

2. S. Min, C. Zhao, Z. Zhang, G. Chen, X. Qian and Z. Guo, J. Mater. Chem. A, 2015, 3, 3641-3650.

3. H. Yi, H. Wang, Y. Jing, T. Peng, Y. Wang, J. Guo, Q. He, Z. Guo and X. Wang, J. Mater. Chem. A, 2015, 3, 19545-19555.

4. S. Liu, S. C. Lee, U. Patil, I. Shackery, S. Kang, K. Zhang, J. H. Park, K. Y. Chung and S. C. Jun, J. Mater. Chem. A, 2017, 5, 1043-1049.

5. F. Cao, G. Pan, X. Xia, P. Tang and H. Chen, J. Power Sources, 2014, 264, 161-167.

6. Y. Jiao, Y. Liu, B. Yin, S. Zhang, F. Qu and X. Wu, Nano Energy, 2014, 10, 90-98.

7. D. Cai, B. Liu, D. Wang, L. Wang, Y. Liu, H. Li, Y. Wang, Q. Li and T. Wang, J. Mater. Chem. A, 2014, 2, 4954-4960.

8. W. Fu, Y. Wang, W. Han, Z. Zhang, H. Zha and E. Xie, J. Mater. Chem. A, 2016, 4, 173-182.

9. J. Yang, C. Yu, X. Fan, S. Liang, S. Li, H. Huang, Z. Ling, C. Hao and J. Qiu, Energy Environ. Sci., 2016, 9, 1299-1307.

10. B. Liu, D. Kong, Z. X. Huang, R. Mo, Y. Wang, Z. Han, C. Cheng and H. Y. Yang, Nanoscale, 2016, 8, 10686-10694.

11. Y. Zhao, L. Hu, S. Zhao and L. Wu, Adv. Funct. Mater., 2016, 26, 4085–4093

12. F. Lai, Y. E. Miao, L. Zuo, H. Lu, Y. Huang and T. Liu, Small, 2016, 12, 3235–3244.

13. C. Xia, Q. Jiang, C. Zhao, P. M. Beaujuge and H. N. Alshareef, Nano Energy, 2016, 24, 78-86.

14. D. Du, R. Lan, W. Xu, R. Beanland, H. Wang and S. Tao, J. Mater. Chem. A, 2016, 4, 17749-17756.

15. J. Chen, J. Xu, S. Zhou, N. Zhao and C.-P. Wong, Nano Energy, 2016, 21, 145-153.